2010

Interionic Energy Transfer in $Y_3Al_5O_{12}$: Ce^{3+}, Pr^{3+} Phosphor

Lei Wang
Chinese Academy of Sciences

Xia Zhang
Chinese Academy of Sciences

Zhendong Hao
Chinese Academy of Sciences

Yongshi Luo
Chinese Academy of Sciences

Jiahua Zhang
Chinese Academy of Sciences

See next page for additional authors

Authors
Lei Wang, Xia Zhang, Zhendong Hao, Yongshi Luo, Jiahua Zhang, and Xiao-Jun Wang

Interionic energy transfer in $Y_3Al_5O_{12}:Ce^{3+}$, Pr^{3+} phosphor

Lei Wang,[1,2] Xia Zhang,[1] Zhendong Hao,[1] Yongshi Luo,[1] Jiahua Zhang,[1,a)] and Xiao-jun Wang[3]
[1]*Key Laboratory of Excited State Processes, Changchun Institute of Optics, Fine Mechanics and Physics, Chinese Academy of Sciences, 3888 Eastern South Lake Road, Changchun 130033, China*
[2]*Graduate School, Chinese Academy of Sciences, Beijing, 100039, China*
[3]*Department of Physics, Georgia Southern University, Statesboro, Georgia 30460, USA*

(Received 5 July 2010; accepted 8 September 2010; published online 9 November 2010)

We present an investigation of dynamical processes of nonradiative energy transfer (ET) between Ce^{3+} and Pr^{3+}, and between Pr^{3+} ions in $Y_3Al_5O_{12}:Ce^{3+}$, Pr^{3+} phosphor. Photoluminescence spectroscopy and fluorescence decay patterns are studied as a function of Pr^{3+} and Ce^{3+} concentrations. The analysis based on Inokuti–Hirayama model indicates that the ET from the lowest $5d$ state of Ce^{3+} to the $^1D_2$ state of Pr^{3+}, and the quenching of the $^1D_2$ state through a cross relaxation involving Pr^{3+} ions in the ground state are both governed by electric dipole–dipole interaction. An increase in the Ce^{3+}–Pr^{3+} ET rate followed by the enhanced red emission line of Pr^{3+} relative to the yellow emission band of Ce^{3+} on only increasing Ce^{3+} concentration is observed. This behavior is attributed to the increase in the spectral overlap integrals between Ce^{3+} emission and Pr^{3+} excitation due to the fact that the yellow band shifts to the red spectral side with increasing Ce^{3+} concentration while the red line dose not move. For Ce^{3+} concentration of 0.01 in $YAG:Ce^{3+}$, Pr^{3+}, the rate constant and critical distance are evaluated to be 4.5×10^{-36} $cm^6\ s^{-1}$, 0.81 nm for Ce^{3+}–Pr^{3+} ET and 2.4×10^{-38} $cm^6\ s^{-1}$, 1.30 nm for Pr^{3+}–Pr^{3+} ET. Spectroscopic study also demonstrates a pronounced ET from the lowest $4f5d$ of Pr^{3+} to the $5d$ of Ce^{3+}. A proportional dependence of the initial transfer rate on acceptor concentration is observed in each of these ET pathways. The proportional coefficient as the averaged ET parameters for initial decay are determined, meaning the ET efficiency for the same concentration of acceptors follows the order of Pr^{3+}–Pr^{3+} > Pr^{3+}–Ce^{3+} > Ce^{3+}–Pr^{3+}. © *2010 American Institute of Physics*.
[doi:10.1063/1.3500458]

I. INTRODUCTION

Solid-state lighting based on white light-emitting diodes (LEDs) has attracted much interest in recent years due to its advantages of low applied voltage, long life, small size, and absence of mercury. At present, the main strategy for producing white light is combine blue LED with the yellow emitting $Y_3Al_5O_{12}:Ce^{3+}$ ($YAG:Ce^{3+}$) phosphor, which can strongly absorb the blue light and subsequently emit yellow light, originating from the transition from the lowest $5d$ state to the $^2F_{5/2}$ and $^2F_{7/2}$ ground states of Ce^{3+}.[1,2] However, $YAG:Ce^{3+}$ has relatively weak emission in red spectral region, leading to low color rendering index for current white LEDs. To enhance the red component, Mueller-Mach *et al.*[3] added Pr^{3+} into $YAG:Ce^{3+}$ and consequently obtained additional sharp red line at about 608 nm, originating from $^1D_2 \rightarrow {}^3H_4$ transition of Pr^{3+}, as only Ce^{3+} is excited by blue light at around 470 nm. The appearance of the red emission line of Pr^{3+} implies the performance of energy transfer (ET) from Ce^{3+} to Pr^{3+} in $YAG:Ce^{3+}$, Pr^{3+}. Subsequently, many studies on optical properties of $YAG:Ce^{3+}$, Pr^{3+} were made.[4–7] Further increasing Pr^{3+} concentration for obtaining enough red components to meet the requirement of white LEDs with high color rendering, however, the red line decreases due to self concentration quenching.[5,6] In the present work, we observe that the red line can be continuously enhanced by increasing Ce^{3+} concentration as the quenching of the red line takes place. Besides Ce^{3+}–Pr^{3+} ET, there also exists Pr^{3+}–Ce^{3+} ET in $YAG:Ce^{3+}$, Pr^{3+},[6] reflecting a mutual ET system. Studies show that various ET processes play an important role on optical properties of $YAG:Ce^{3+}$, Pr^{3+}. To optimize the phosphor by controlling the concentrations of Ce^{3+} and Pr^{3+} in YAG, it is therefore significant to understand the dynamical processes of ET between the dopant ions, which to our knowledge have not been studied in detail. For Ce^{3+}–Pr^{3+} ET, the main pathway is conformably considered to start from the lowest $5d$ state of Ce^{3+} to the $^1D_2$ state of Pr^{3+}. Based on the Ce^{3+} and Pr^{3+} energy level diagrams, a radiative ET seems to be possible. However, we cannot observe the red line in a blend of $YAG:Ce^{3+}$ and $YAG:Pr^{3+}$ phosphors, indicating that the ET takes place rather by nonradiative interaction, as suggested by Yang and Kim.[6] In this case, Inokuti–Hirayama model is valid.

In this paper, we demonstrate various transfer pathways and transfer dynamical processes in Pr^{3+} and Ce^{3+} codoped YAG basing on the experimental measurements of photoluminescence (PL), photoluminescence excitation (PLE) spectra, and fluorescence decay curves. Moreover, the ET from Pr^{3+} to Ce^{3+} is also studied. The relative PL intensities of Ce^{3+} and Pr^{3+} as a function of Ce^{3+} and Pr^{3+} concentrations are analyzed, exhibiting a good agreement with the results evaluated from fluorescence decay data.

[a)]Electronic mail: zhangjh@ciomp.ac.cn.

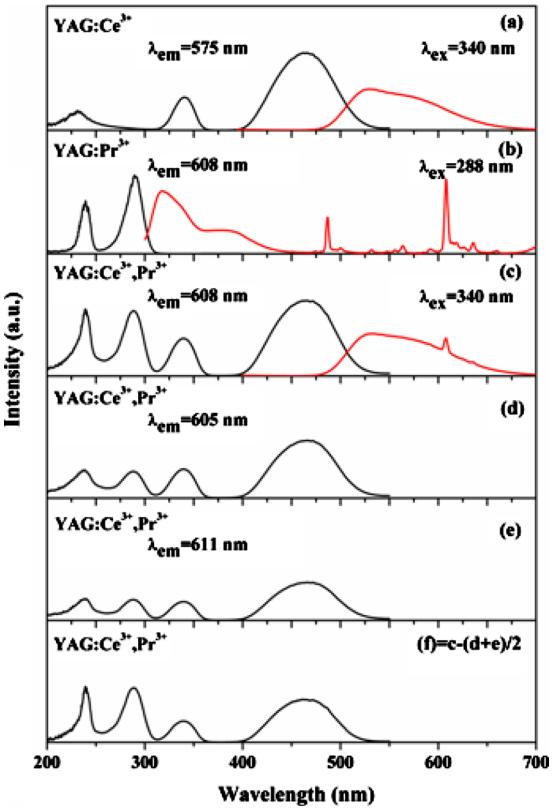

FIG. 1. (Color online) PL and PLE spectra of $(Y_{0.99}Ce_{0.01})_3Al_5O_{12}$, $(Y_{0.995}Pr_{0.005})_3Al_5O_{12}$ and $(Y_{0.985},Ce_{0.01}Pr_{0.005})_3Al_5O_{12}$.

II. EXPERIMENTAL

The powder samples have been prepared by conventional solid-state reaction.Y_2O_3, CeO_2, Al_2O_3, and Pr_6O_{11} are mixed in a molar of $(Y_{1-x-y}Ce_xPr_y)_3Al_5O_{12}$ (x, y represent the concentration of Ce^{3+} and Pr^{3+}, respectively), 3 wt% BaF_2 has been added to as the flux. After a good mixing in an agate mortar, the mixture has been sintered at 1500 °C for 3 h under a reducing atmosphere. The structure of the final products is characterized by power x-ray diffraction (XRD). The XRD patterns are in good agreement with Joint Committee for Powder Diffraction Standard file 33-040 for YAG. No additional XRD peaks are found, indicating that the dopant ions do not change the structure of the YAG host. PL and PLE spectra are measured at room temperature with a Hitachi Spextra-fluorometer (F-4500). The decay of the fluorescence from Ce^{3+} is measured by an FL920 fluorimeter (Edinburgh Instruments, Livingston, U.K.) with a hydrogen flash lamp (nF900; Edinburgh Instruments). In the measurements of the fluorescent decay of Pr^{3+}, an optical parametric oscillator is used as an excitation source. The signal is detected by a Tektronix digital oscilloscope (TDS 3052).

III. RESULTS AND DISCUSSION

A. Spectroscopic evidence of ET

Figure 1 shows the PL and PLE spectra of three samples, namely Ce^{3+} singly doped $(Y_{0.99}Ce_{0.01})_3Al_5O_{12}$ (a), Pr^{3+} singly doped $(Y_{0.995}Pr_{0.005})_3Al_5O_{12}$ (b), and Ce^{3+}, Pr^{3+} doubly doped $(Y_{0.985}Ce_{0.01}Pr_{0.005})_3A_{15}O_{12}$ (c), respectively. The Ce^{3+} singly doped sample exhibits a well known yellow emitting broad band due to the transition from the lowest-lying $5d$ state to the $4f$ ground state, peaking at around 530 nm. The PLE spectrum of the yellow band consists of a group of PLE bands, including a blue PLE band at 470 nm corresponding to the transition from the ground state to the lowest-lying $5d$ state, and two ultraviolet (UV) PLE bands corresponding to the upper $5d$ states, located at 340 nm and 230 nm, respectively,[1,2] as shown in Fig. 1(a). The Pr^{3+} singly doped sample exhibits three groups of emission of Pr^{3+} upon 288 nm excitation, as shown in Fig. 1(b). The group in the UV region consists of two strong bands located at 317 nm and 381 nm, which are originated in the transitions from the lowest-lying $4f5d$ state to ^3H_J (J=4,5,6) and ^3F_J (J=2,3,4) states, respectively.[8] The group in the range of 450–600 nm originates from $^3P_0 \rightarrow {}^3H_{4,5}$ transitions dominated by a intense blue emission line at 488 nm due to $^3P_0 \rightarrow {}^3H_4$ transition. Another group in red originates from $^1D_2 \rightarrow {}^3H_4$ transitions dominated by a intense red emission line at 608 nm with a weak satellite line at 640 nm.[9,10] The PLE spectra of the three groups of emission in Pr^{3+} singly doped sample are identical in the UV spectral range, showing two $4f5d$ PLE bands located at 288 nm and 238 nm, respectively. In Fig. 1(c), the PL spectrum of Ce^{3+} and Pr^{3+} doubly doped sample contains not only the yellow band of Ce^{3+} but also the intense red lines of Pr^{3+} when only Ce^{3+} is excited at 340 nm, demonstrating occurrence of ET from Ce^{3+} to Pr^{3+}. To further exam the ET in the doubly doped sample, the PLE spectrum of the pure 608 nm red line is obtained, as shown in Fig. 1(f), by subtracting the PLE spectrum monitoring the feet of the 608 nm lines from that in Fig. 1(c) monitoring the peak of the 608 nm lines. The PLE spectrum of the feet of the 608 nm line is obtained by averaging that monitoring 605 nm and 611 nm, as shown in Figs. 1(d) and 1(e), respectively. It is clearly presented that the PLE spectrum of the pure 608 nm emission line of Pr^{3+}, as shown in Fig. 1(f) contains the strong blue and the UV PLE bands of Ce^{3+}, which are absent in Pr^{3+} singly doped sample. As a result, ET from Ce^{3+} to Pr^{3+} is evident.

Moreover, it is also observed in Figs. 1(d) and 1(e) that the PLE spectra monitoring at 605 and 611 nm within the broad emission band of Ce^{3+} appear the strong UV PLE band of Pr^{3+} at 288 nm. This indicates a pronounced ET from the lowest-lying $4f5d$ state of Pr^{3+} to the $5d$ state of Ce^{3+}.

B. Ce^{3+}–Pr^{3+} ET

Figure 2 shows the PL spectra of sample series A $(Y_{0.99-x}Ce_{0.01}Pr_x)_3Al_5O_{12}$ with a fixed Ce^{3+} concentration at 0.01 and various Pr^{3+} concentration x in the range of 0–0.02. In order to avoid direct excitation into the ^3P_J (J=0,1,2) levels of Pr^{3+}, we do not use 470 nm as an excitation to populate the lowest-lying $5d$ state of Ce^{3+}, instead we use 340 nm to excite the upper $5d$ state of Ce^{3+}. Besides a rapid relaxation down to the lowest $5d$ state, the excited upper $5d$ state of Ce^{3+} may have additional two possible pathways for deexcitation, which are radiative transition to the ground state and ET to the ^3P_J states of Pr^{3+}. In our experiments, a weak purple emission band from the upper $5d$ state was indeed observed at about 380 nm. However, the $^3P_0 - {}^3H_4$ blue

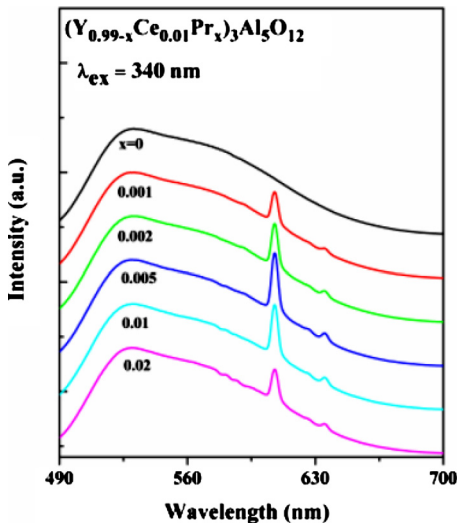

FIG. 2. (Color online) PL spectra of $(Y_{0.99-x}Ce_{0.01}Pr_x)_3Al_5O_{12}$, (x =0–0.02) under 340 nm excitation. The intensity of the yellow band in each spectrum is normalized.

emission line of Pr^{3+} was not detected at 488 nm for various x values. This behavior indicates that the pathway of Ce^{3+}–Pr^{3+} ET hardly starts from both of the upper 5*d* state and the lowest 5*d* state of Ce^{3+} to the $^3P_0$ level of Pr^{3+}, as illustrated in Fig. 3. This conclusion is also supported by the fact that both the purple and yellow emission bands of Ce^{3+} do not spectrally overlap with the $^3H_4$–^3P_J absorption lines of Pr^{3+} in the blue spectral region. The appearance of the red emission line of Pr^{3+} for $x>0$ is therefore, the result of ET from the lowest 5*d* of Ce^{3+} to the $^1D_2$ of Pr^{3+} because the yellow emission band of Ce^{3+} has a spectral overlap with the red line (zero-phonon line) of Pr^{3+}. Basing on this ET pathway, we focus our study on the PL integrated intensity ratio of the red line from Pr^{3+} as an acceptor to the yellow band from Ce^{3+} as a donor because a large red/yellow ratio is significant for fabricating white LEDs with high color rendering index. In Fig. 2, where the intensity of the yellow band is normalized in each PL spectrum, it is observed that the red line grows up with increasing x until it reaches the

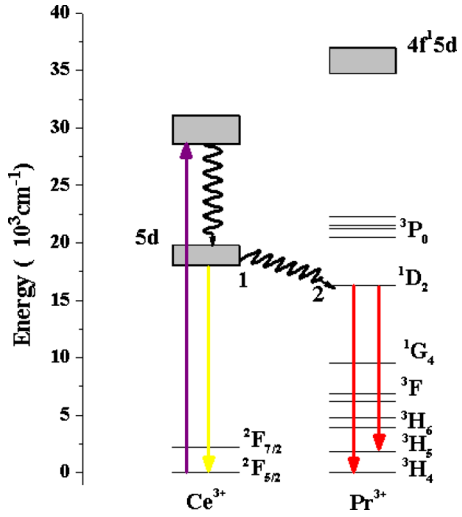

FIG. 3. (Color online) Energy level diagrams of Ce^{3+} and Pr^{3+} with the indicated pathway of $Ce^{3+}\rightarrow Pr^{3+}$ ET.

maximum at x around 0.005. Subsequently, the red line falls down with further increasing x. The growth of the red line naturally implies the increase in the efficiency of Ce^{3+}–Pr^{3+} ET. The decrease for x higher than 0.005 is attributed to concentration self-quenching by another Pr^{3+} in the ground state through a cross relaxation, as described by $(^1D_2, ^3H_4)$ $-(^1G_4, ^3F_4)$.[11,12] The quenching has been proved by the observation of rapid shortening of the $^1D_2$ lifetime with increasing x, as described in Sec. III C. If the red/yellow ratio is governed by Ce^{3+}–Pr^{3+} ET and self-quenching of Pr^{3+}, each value of the ratio relates to the corresponding fluorescence lifetimes of Ce^{3+} and Pr^{3+}. In donor-acceptor ET system, due to nonexponential decay of donor fluorescence intensity $I_D(t)$ in the presence of acceptors, we define an average fluorescence lifetime of the donors as

$$\langle \tau_D \rangle = \int_0^\infty I_D(t)dt, \tag{1}$$

where $I_D(t)$ is normalized to its initial intensity. The luminescence efficiency of the donors is given by $\eta_D = \langle \tau_D \rangle / \tau_{D0}$ with τ_{D0} being the intrinsic lifetime of the donor fluorescence. In the absence of acceptors, the $\langle \tau_D \rangle$ especially labeled by $\langle \tau_D \rangle_0$ is equal to τ_{D0} if the donor concentration is sufficient low, otherwise $\langle \tau_D \rangle$ may be less than τ_{D0} due to various nonradiative quenching processes induced by donors. If $\langle \tau_D \rangle_0^{-1} - \tau_{D0}^{-1} \ll \tau_{D0}^{-1}$, i.e., the donor induced quenching rate much less than the radiative rate, the fluorescence still keeps an exponential decay in the time scale of τ_{D0}. In this case, the efficiency of donor-acceptor ET is then written as $\eta_{DA} = 1 - \langle \tau_D \rangle / \langle \tau_D \rangle_0$. The luminescence efficiency of acceptors is given by $\eta_A = \langle \tau_A \rangle / \tau_{A0}$ with $\langle \tau_A \rangle$ and τ_{A0} being the average and intrinsic fluorescence lifetimes for the acceptors, respectively. In continuous excitation of donors, the PL intensity ratio of the acceptors to the donors is then expressed by

$$\frac{I_A}{I_D} = \frac{\eta_{DA}\eta_A}{\eta_D} = \left(\frac{1}{\langle \tau_D \rangle} - \frac{1}{\langle \tau_D \rangle_0} \right) \langle \tau_A \rangle \frac{\tau_{D0}}{\tau_{A0}}, \tag{2}$$

where the term $(1/\langle \tau_D \rangle - 1/\langle \tau_D \rangle_0)$ is the macroscopic ET rate. Equation (2) indicates that in ET system the PL intensity ratio changes synchronously with the value of $(1/\langle \tau_D \rangle - 1/\langle \tau_D \rangle_0)\langle \tau_A \rangle$, which can be calculated using the measured values of the average lifetimes of the donor and the acceptor fluorescence. To test the validity of Eq. (2) in YAG:Ce^{3+}, Pr^{3+}, we have measured the decay curves of the yellow fluorescence of Ce^{3+} and the red fluorescence of Pr^{3+} for different x in sample series A, as shown in Figs. 4 and 5, respectively. The decay of the yellow fluorescence is measured by monitoring at 530 nm upon 340 nm pulsed excitation and that of the red fluorescence by monitoring $^1D_2 \rightarrow {}^3H_5$ emission of Pr^{3+} at 714 nm upon $^3H_4 \rightarrow {}^1D_2$ pulsed excitation at 608 nm. The average lifetimes obtained from these decay patterns are listed in Table I. It is found that the decay of the red fluorescence speeds up rapidly with increasing x, indicating a strong self-quenching. Labeling the emitting state of the donor Ce^{3+} by 1 and that of the acceptor Pr^{3+} by 2, the x dependence of the red/yellow ratio (I_2/I_1) obtained from PL spectra and that calculated using $(1/\langle \tau_1 \rangle - 1/\langle \tau_1 \rangle_0)\langle \tau_2 \rangle$ are both plotted in Fig. 6, clearly demonstrating their identical x

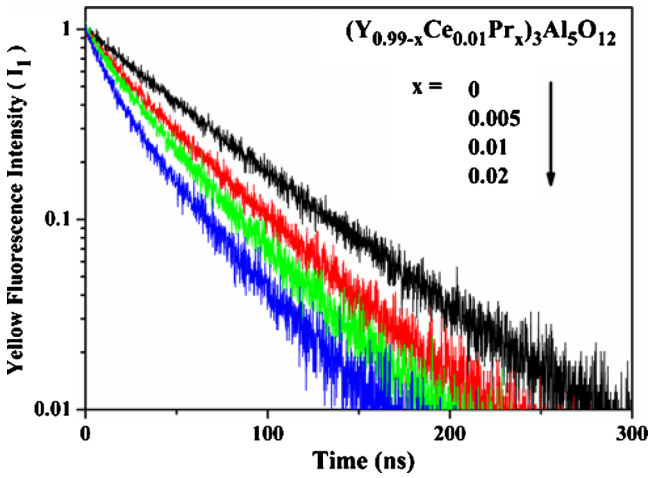

FIG. 4. (Color online) Decay curves of the yellow fluorescence in $(Y_{0.99-x}Ce_{0.01}Pr_x)_3Al_5O_{12}$ for x=0, 0.005, 0.01, and 0.02.

dependence so that proportional relationship as described in Eq. (2).

The maximum of the ratio appears at around x=0.005, which relates to concentration quenching of Pr^{3+} in $(Y_{0.99-x}Ce_{0.01}Pr_x)_3Al_5O_{12}$ for its red fluorescence. For practical use of the white LED phosphor, the x dependence of the absolute PL intensities is an important parameter for optimizing the phosphors. We have experimentally observed that the overall PL intensities decrease with increasing x due to continuous reduction of the emission efficiency of the $^1D_2$ level through the cross relaxation as mentioned above. If the strongest red line is required instead of the red/yellow ratio, we must analyze the absolute intensity of the red line that is written as $\eta_{DA}\eta_A$. Comparing to the red/yellow ratio expressed as $\eta_{DA}\eta_A/\eta_D$, the maximum of $\eta_{DA}\eta_A$ should occur at x below 0.005 because the value of η_D reduces with increasing x. For $x<0.005$, the loss of the overall PL intensity is estimated to be less than 0.1 using the lifetimes listed in Table I. The self-quenching strongly limits the maximal value of the red/yellow ratio and the absolute intensity of the red line. Fortunately, the enhancement of this ratio has been

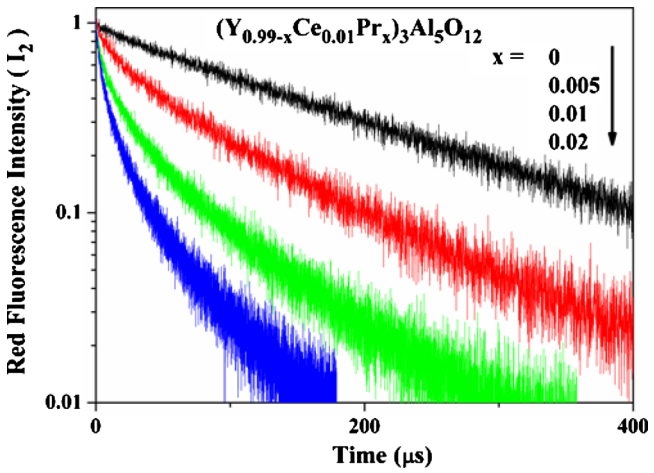

FIG. 5. (Color online) Decay curves of the red line in $(Y_{0.99-x}Ce_{0.01}Pr_x)_3Al_5O_{12}$ for x=0, 0.005, 0.01, and 0.02.

TABLE I. Fluorescent lifetimes and transfer efficiencies in $(Y_{0.99-x}Ce_{0.01}Pr_x)_3Al_5O_{12}$.

x	Ce^{3+} 5*d*, τ_{10}=61 ns, $\langle\tau_1\rangle$ (ns), λ_{ex}=340 nm	Pr^{3+} $^1D_2$, τ_{20}=202 μs, $\langle\tau_2\rangle$ (μs), λ_{ex}=608 nm	η_{12}
	λ_{em}=530 nm	λ_{em}=714 nm	
0	57.8	202	0
0.001	53.4	162	0.08
0.002	51.0	141	0.12
0.005	46.0	90	0.20
0.01	42.1	59	0.27
0.02	30.3	20	0.48

performed by increasing Ce^{3+} concentration, which will be demonstrated in Sec. III D.

The decays in Figs. 4 and 5 change from exponential to nonexponential patterns with increasing x, reflecting the effect of ET The normalized intensity of the donor fluorescence can be written as

$$I_D(t) = I_{D0}(t)f(t), \tag{3}$$

where $I_{D0}(t)$ is the decay function of donors in the absence of acceptors, the function $f(t)$ characterizes the loss of excited donors due to one way ET to the acceptors. If ET rate between a donor and an acceptor is proportional to an inverse power of the distance r, writing as α/r^m, according to Inokuti–Hirayama formula,[13] we have

$$f(t) = \exp\left[-\frac{4}{3}\pi\Gamma\left(1-\frac{3}{m}\right)n_A\alpha^{3/m}t^{3/m}\right], \tag{4}$$

where α is a rate constant for ET. $m=6,8,10$, the coefficient for dipole-dipole, dipole-quadrupole, and quadrupole-quadrupole interaction, respectively. n_A is the number of acceptor ions per unit volume. From Eqs. (3) and (4), $\log\{\ln[I_{D0}(t)/I_D(t)]\}$ acts as a linear function of $\log(t)$ with a slope of $3/m$, and $\ln[I_D(t)/I_{D0}(t)]$ is proportional to $t^{3/m}$ with

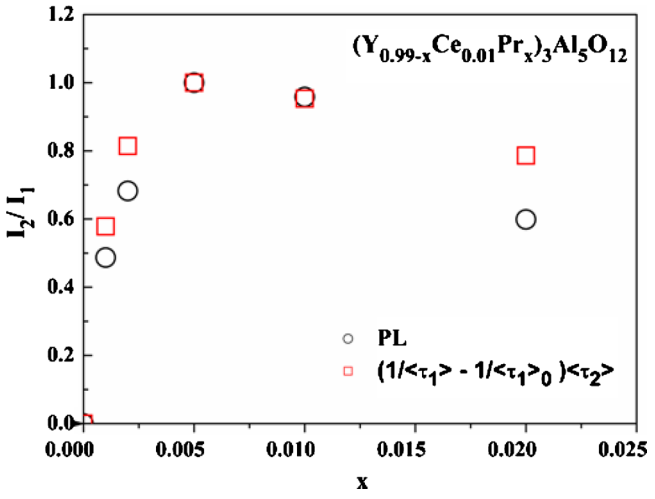

FIG. 6. (Color online) x dependence of ratio (I_2/I_1) obtained directly from PL spectra with that evaluated using $(1/\langle\tau_1\rangle - 1/\langle\tau_1\rangle_0)\langle\tau_2\rangle$ for samples $(Y_{0.99-x}Ce_{0.01}Pr_x)_3Al_5O_{12}$, (x=0–0.02). The maximal value of the ratio is normalized.

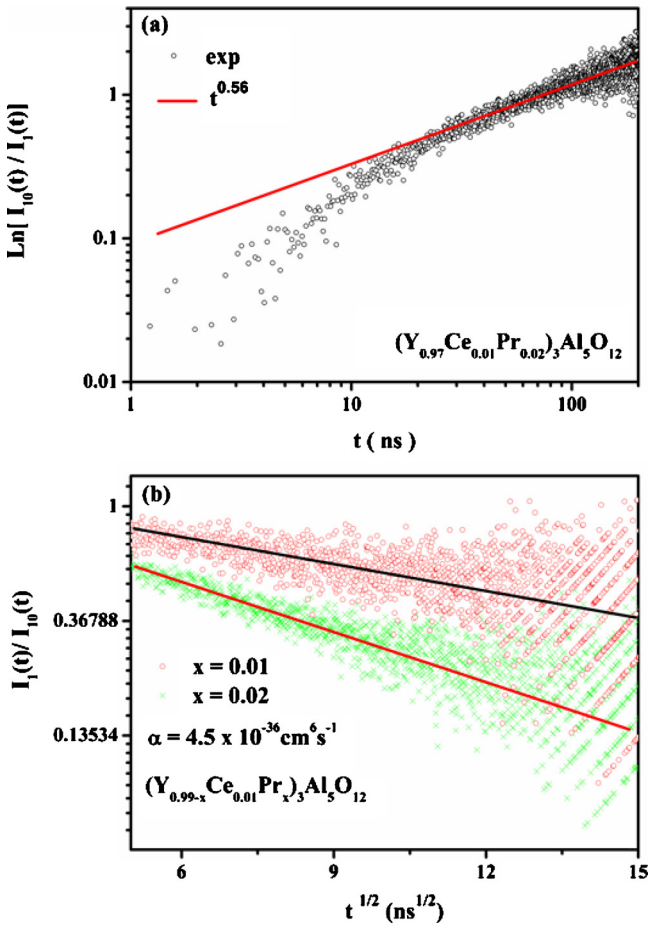

FIG. 7. (Color online) log-log plot of $\ln[I_{10}(t)/I_1(t)]$ vs t for sample $(Y_{0.99-x}Ce_{0.01}Pr_x)_3Al_5O_{12}$ with x=0.02 (a) and plotted $\ln[I_1(t)/I_{10}(t)]$ vs $t^{1/2}$ for the samples $(Y_{0.99-x}Ce_{0.01}Pr_x)_3Al_5O_{12}$ with x=0.01 and 0.02 (b). The solid lines indicate the fitting behaviors.

a slope of $-4\pi\Gamma(1-3/m)n_A\alpha^{3/m}/3$. Figure 7(a) shows the log-log plot of $\ln[I_{10}(t)/I_1(t)]$ versus t for sample $(Y_{0.99-x}Ce_{0.01}Pr_x)_3Al_5O_{12}$ with x=0.02. It is demonstrated that the slope for $t>20$ ns is 0.56 more close to 1/2, indicating an electric dipole-dipole interaction for ET. Regarding m as 6, we have plotted $\ln[I_1(t)/I_{10}(t)]$ versus $t^{1/2}$ for the samples $(Y_{0.99-x}Ce_{0.01}Pr_x)_3Al_5O_{12}$ with x=0.01 and 0.02, as shown in Fig. 7(b). The best fitting to each of the two curves yields a transfer constant $\alpha=4.5\times10^{-36}$ cm^6 s^{-1}. In the fitting n_A, i.e., the number density of Pr^{3+}, is given by xN_Y with $N_Y=1.38\times10^{22}$ cm^{-3} being the number of Y sites per unit volume in YAG. Using the value of α, the critical ET distance r_0 (the spatial separation between a donor and an acceptor where the ET rate $\alpha/r_0^6=1/\tau_{10}$) is calculated to be about 0.81 nm. In the calculation, the intrinsic lifetime τ_{10} is 61 ns determined in 0.0005 Ce^{3+} lowly doped YAG, which exhibits a pure exponential decay.

In Fig. 7(a) there is an increase in slope below 20 ns, forming a crossover.[14] As we know, Eq. (4) is obtained by assuming the nearest distance between a donor and an acceptor to be 0, leading to an infinite initial ET rate. Hence, Eq. (4) is not applicable at short times which is less than 20 ns in the present sample. In the case of discrete lattices, the initial ET rate is described by[15]

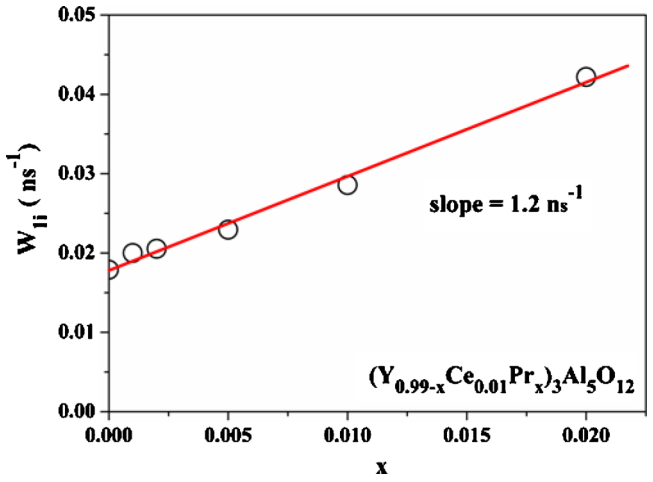

FIG. 8. (Color online) Dependence of W_{1i} on x in $(Y_{0.99-x}Ce_{0.01}Pr_x)_3Al_5O_{12}$ (x=0–0.02)

$$W_{DAi}=x\sum_l w_{0l}, \tag{5}$$

where w_{0l} is the ET rate from a donor at site 0 to an acceptor at site l excluding $l=0$. The function $f(t)$, therefore, exhibits a linear behavior $\{f(t)\approx\exp[-W_{DAi}t]\}$ at short times[16] and a $t^{3/m}$ variation at longer times. In random distribution of acceptors in host lattices $\Sigma_l w_{0l}$ is the averaged ET parameter, denoting the total ET rate of a donor ion embedded within a complete acceptor environment (x=1). In the present work, the sample for x=0 shows an exponential decay of fluorescence. Therefore, $\Sigma_l w_{0l}$ can be experimentally obtained by using the following linear relationship with the initial decay rate W_{Di} of the donor fluorescence[17]

$$W_{Di}=x\sum_l w_{0l}+\langle\tau_D\rangle_0^{-1}. \tag{6}$$

Figure 8 shows a linear dependence of W_{1i} on x in sample series A $(Y_{0.99-x}Ce_{0.01}Pr_x)_3Al_5O_{12}$ (x=0–0.02). The slope gives the value of $\Sigma_l w_{0l}$ to be around 1.2 ns^{-1}, yielding $\tau_{10}\Sigma_l w_{0l}$ to be 73, where $\tau_{10}=61$ ns.

C. Pr^{3+}–Pr^{3+} ET

The decay patterns of Pr^{3+} $^1D_2$ are analyzed in sample series A to understand the self-quenching through a cross relaxation, as described by $(^1D_2,{}^3H_4)-(^1G_4,{}^3F_4)$. The log-log plot of $\ln[I_{20}(t)/I_2(t)]$ versus t for sample $(Y_{0.99-x}Ce_{0.01}Pr_x)_3Al_5O_{12}$ with x=0.02 is shown in Fig. 9(a). The $I_{20}(t)$ is an pure exponential decay function $\exp(-t/\tau_{20})$ with $\tau_{20}=202$ μs being the intrinsic lifetime of the $^1D_2$ level of Pr^{3+} in YAG obtained from the tail decay of the fluorescence in 0.001 Pr^{3+} doped YAG. The slope for $t>10$ μs is more close to 0.5, indicating an electric dipole-dipole ET between Pr^{3+} ions. The linear dependence of $\ln[I_2(t)/I_{20}(t)]$ versus $t^{1/2}$ are observed and a good agreement between the theoretical and experimental results are performed for various x when fixing the rate constant α to be 2.4×10^{-38} cm^6 s^{-1} for Pr^{3+}–Pr^{3+} self-quenching, as shown in Fig. 9(b). The critical quenching distance of 1.3 nm is evaluated. Meanwhile, the linear dependence of the initial

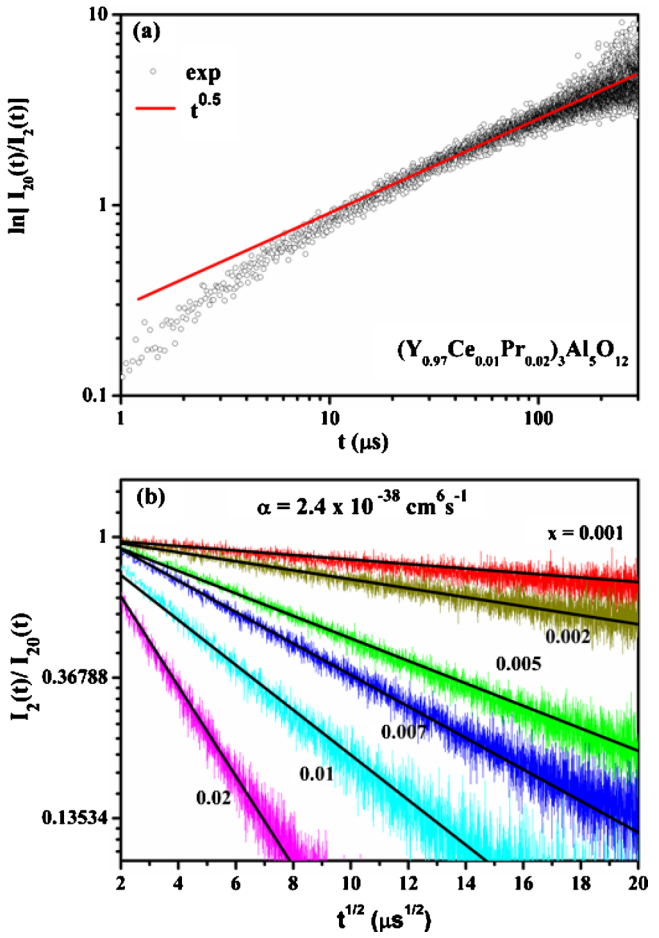

FIG. 9. (Color online) log-log plot of $\ln[I_{20}(t)/I_2(t)]$ vs t for sample $(Y_{0.99-x}Ce_{0.01}Pr_x)_3Al_5O_{12}$ with x=0.02 (a) and plotted $\ln[I_2(t)/I_{20}(t)]$ vs $t^{1/2}$ for the samples $(Y_{0.99-x}Ce_{0.01}Pr_x)_3Al_5O_{12}$ with various x (x=0–0.02) (b). The solid lines indicate the fitting behaviors.

decay rate of the red fluorescence W_{2i} on x, as shown in Fig. 10, gives the value of $\Sigma_l w_{0l}$ to be 6.2 μs^{-1}, yielding $\tau_{20}\Sigma_l w_{0l}$ to be 1252, which is a order of magnitude larger than 73 for Ce^{3+}–Pr^{3+} ET. This indicates that the self-quenching of Pr^{3+} $^1D_2$ by another Pr^{3+} in the ground state is more efficient than the Ce^{3+} $5d$–Pr^{3+} $^1D_2$ ET.

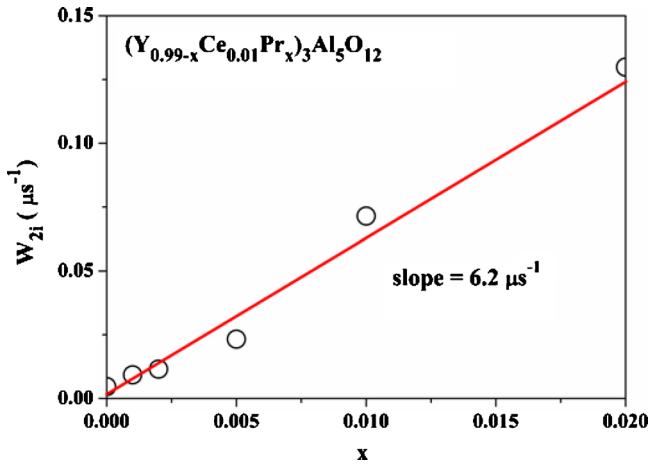

FIG. 10. (Color online) Dependence of W_{2i} on x in $(Y_{0.99-x}Ce_{0.01}Pr_x)_3Al_5O_{12}$ (x=0–0.02)

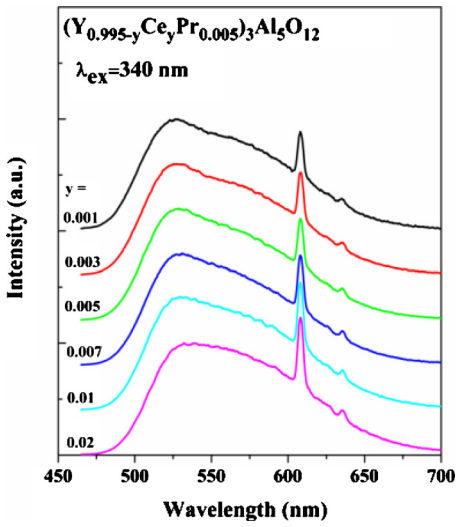

FIG. 11. (Color online) PL spectra of $(Y_{0.995-y}Ce_yPr_{0.005})_3Al_5O_{12}$, (y =0–0.02) upon 340 nm excitation, where the intensity of the yellow band in each spectrum is normalized.

D. Ce^{3+}–Pr^{3+} ET versus Ce^{3+} concentration

In this section, we demonstrate the study on enhancing the red/yellow ratio by increasing Ce^{3+} concentration instead of Pr^{3+} to avoid concentration quenching. Figure 11 shows the PL spectra of sample series B $(Y_{0.995-y}Ce_yPr_{0.005})_3Al_5O_{12}$ with Pr^{3+} concentration fixing at 0.005 and various Ce^{3+} concentration y in the range of 0–0.02. When the intensity of the yellow emission band of Ce^{3+} is normalized, it is found that the red emission line of Pr^{3+} monotonously grows up with increasing y. As y=0.02, the ratio is higher than that for x =0.01, i.e., higher than the maximal ratio in sample series A demonstrated in section B. In view of small changes in the red fluorescence lifetimes with increasing y (see Table II), the enhanced red line is the indication of increased macroscopic Ce^{3+}–Pr^{3+} ET rate according to Eq. (2). One can find the existence in connection with the enhancement of the red/yellow ratio is a redshift in the yellow PL band with increasing Ce^{3+} concentration, as has been observed in Ce^{3+} singly doped YAG.[18] The redshift enhances the spectral distribution of the yellow band at the position of the red line, which dose not shift with y. As a result, we consider that the redshift is favorable for effectively increasing the spectral overlap integrals between the yellow emission band and the red absorption line, and therefore enhancing the ET rate which is proportional to the spectral overlap integrals between donor emission and acceptor absorption. Due to weak electron-phonon coupling in $4f$ configuration of rare earth ions, the position of the red emission line can be regarded as that of the zero-phonon absorption line. In the case of much narrower red line than the yellow band, their spectral overlap integral is proportional to the spectral intensity of the normalized yellow band at the red line site, I_{1R}. As we plot the red/yellow ratio I_2/I_1 versus $I_{1R}\langle\tau_2\rangle$, they approximately satisfy a proportional relationship, as shown in Fig. 12. Due to low Pr^{3+} concentration in sample series B, the reduction in the yellow fluorescent lifetimes is less than a half of the intrinsic lifetime even for the Ce^{3+} concentration as high as 0.02. Hence, the fluorescent decays are all approximately

TABLE II. Fluorescent lifetimes and transfer efficiencies in $(Y_{0.995-y}Ce_yPr_{0.005})_3Al_5O_{12}$.

Y	Pr^{3+} $4f5d$, τ_{40}=14 ns, $\langle\tau_4\rangle$ (ns) λ_{ex}=288 nm λ_{em}=380 nm	Pr^{3+} $^3P_0$, τ_{30}=14 μs, $\langle\tau_3\rangle$ (μs) λ_{ex}=288 nm λ_{em}=488 nm	Pr^{3+} $^1D_2$, τ_{20}=202 μs, $\langle\tau_2\rangle$ (μs) λ_{ex}=608 nm λ_{em}=714 nm	Ce^{3+} $5d$, τ_{10}=61 ns, $\langle\tau_1\rangle$ (ns) λ_{ex}=340 nm λ_{em}=530 nm	Ce^{3+} $5d$, YAG:yCe^{3+}, $\langle\tau_1\rangle_0$ (ns) λ_{ex}=340 nm λ_{em}=530 nm	η_{12}	η_{41}	η_{31}
0	14	8.8	162			0	0	0
0.001	11.2	7.7	85	53.3	61.0	0.12	0.20	0.13
0.003	9.9	6.8	72	50.7	60.1	0.16	0.30	0.23
0.005	7.9	6.5	82	51.1	59.3	0.14	0.44	0.26
0.007	6.3	5.9	85	48.7	58.4	0.17	0.55	0.33
0.01	⋯	5.4	90	46.0	57.2	0.20	⋯	0.39
0.02	⋯	4.1	90	43.5	53.5	0.19	⋯	0.53

exponential in the time scale of the intrinsic lifetime. It means the initial ET rate governs the macroscopic ET rate in sample series B. As we know the initial ET rate is proportional to the spectral overlap integrals between donor and acceptors, the proportional relationship in Fig. 12 is thus expected.

Another possibility causing the enhanced macroscopic ET rate is related to enhanced donor (Ce^{3+})-donor (Ce^{3+}) energy diffusion as increasing donor concentration.[19] As we know, the diffusion dose not changes the initial decay rate of ET.[20] We observe that the initial decay rate of the yellow fluorescence increases as increasing y with a slope of 0.30 ns^{-1} for y in the present range of 0–0.02, as shown in Fig. 13. While, the initial decay rate of fluorescence in Ce^{3+} singly doped YAG also increases with increasing y, but with a smaller slope, 0.17 ns^{-1}. The enhanced decay in Ce^{3+} singly doped YAG can be resulted from some quenching centers generated by doping Ce^{3+} and the one way ET from the high energy Ce^{3+} ions to the low energy Ce^{3+} ions within the inhomogeously broadened PL spectra for high Ce^{3+} concentration.[21,22] If these ET processes are independent on Pr^{3+} concentration, the difference (0.13 ns^{-1}) between the two slopes reflects the increment of Ce^{3+}–Pr^{3+} ET rate due to the increase in the spectral overlap resulted from the redshift in the yellow band with increasing y. The red/yellow ratio evaluated for various y by using Eq. (2) in relation to the macroscopic ET rates is roughly close to that from PL, as shown in Fig. 12. Using the initial ET rates W_{12i} instead of the macroscopic ET rates, the evaluated red/yellow ratio by $W_{12i}\langle\tau_2\rangle$ dose not change much due to the dominance of the initial ET in the whole ET in the Sample series B. Here, the initial ET rate is calculated using Eq. (6) with the data shown in Fig. 13. The absolute PL intensity reaches the maximum when Ce^{3+} concentration y is about 0.02. In this case, we experimentally found that the optimal concentration of Pr^{3+} occurs at 0.002, which limits the loss of the overall PL intensity less than 0.05 for practical use of the white LED phosphor.

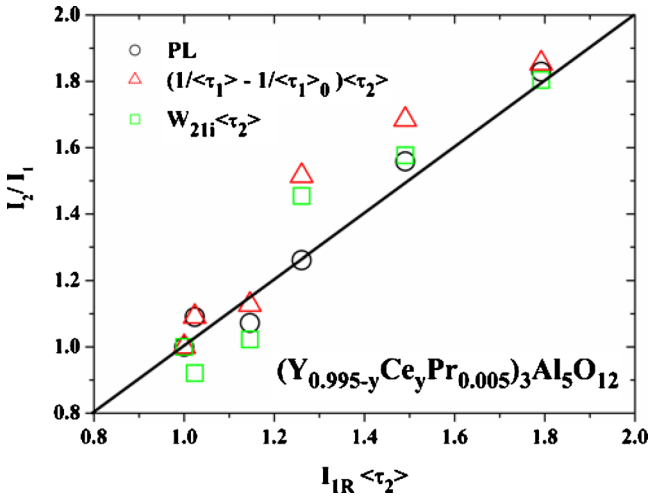

FIG. 12. (Color online) Dependence of ratio (I_2/I_1) on $I_{1R}\langle\tau_2\rangle$, where the ratios obtained directly from PL spectra are compared with that evaluated using $(1/\langle\tau_1\rangle - 1/\langle\tau_1\rangle_0)\langle\tau_2\rangle$ and $W_{21i}\langle\tau_2\rangle$ for samples $(Y_{0.995-y}Ce_yPr_{0.005})_3Al_5O_{12}$ (y=0.001–0.02). The values of both I_2/I_1 and $I_{1R}\langle\tau_2\rangle$ for the lowest y of 0.001 are normalized.

E. Pr^{3+}–Ce^{3+} ET

Figure 14 shows the PL spectra of sample series B $(Y_{0.995-y}Ce_yPr_{0.005})_3Al_5O_{12}$ (y=0–0.02) as the lowest $4f5d$ state of Pr^{3+} is excited at 288 nm, where the UV PL band of Pr^{3+} is normalized. One can find the yellow PL band of Ce^{3+} increases with increasing y, exhibiting the enhanced efficiency of ET from Pr^{3+} to Ce^{3+}. Considering that the lowest $4f5d$ PL bands of Pr^{3+} overlap well with the UV PLE band of Ce^{3+} in the range of 300–400 nm (see Fig. 1), the Pr^{3+}–Ce^{3+} ET may go from the lowest $4f5d$ state (labeled by

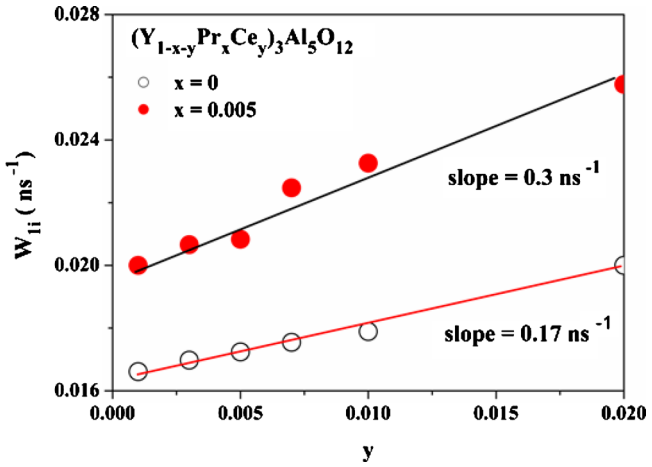

FIG. 13. (Color online) Dependence of W_{1i} on y in $(Y_{0.995-y}Ce_yPr_{0.005})_3Al_5O_{12}$ and $(Y_{1-y}Ce_y)_3Al_5O_{12}$.

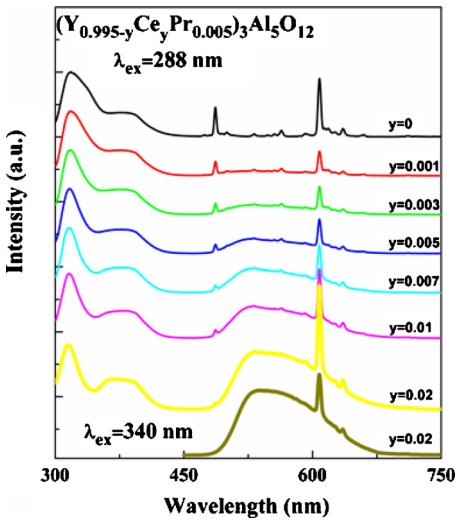

FIG. 14. (Color online) PL spectra of $(Y_{0.995-y}Ce_yPr_{0.005})_3Al_5O_{12}$ (y =0–0.02) upon 288 nm excitation, where the intensity of the yellow band in each spectrum is normalized. A PL spectrum upon 340 nm excitation for y=0.02 is also presented for comparison.

4) of Pr^{3+} to the 5*d* states of Ce^{3+}, as illustrated in Fig. 15. Another possible transfer pathway from Pr^{3+} $^3P_0$ (labeled by 3) to the lowest 5*d* state of Ce^{3+} is also indicated. The $^3P_0$-5*d* transfer has lead to intensity reduction of the $^3P_0 \rightarrow {}^3H_4$ emission line at 488 nm followed by lifetime shortening of the $^3P_0$ level as y is increased. We observed experimentally that the decay for y=0 is purely exponential with a lifetime $\langle\tau_3\rangle_0$ of about 8.8 μs. Ozen *et al.*[19] has measured the decay of $^3P_0$ level in YAG:Pr^{3+} at 20 k and obtained the intrinsic lifetime to be 14 μs is. They proved that the shortening of the lifetime at room temperature is due to enhanced multiphonon relaxation to the lower state $^1D_2$ and therefore this process dose not change its exponential decay behavior. It should be noted that the lifetime of the $^3P_0$ decreases from 8.8 to 4.1 μs, only reducing a half of the $\langle\tau_3\rangle_0$ with increasing y up to 0.02, as listed in Table II. However, the intensity of the blue PL line reduces faster than its lifetime and almost

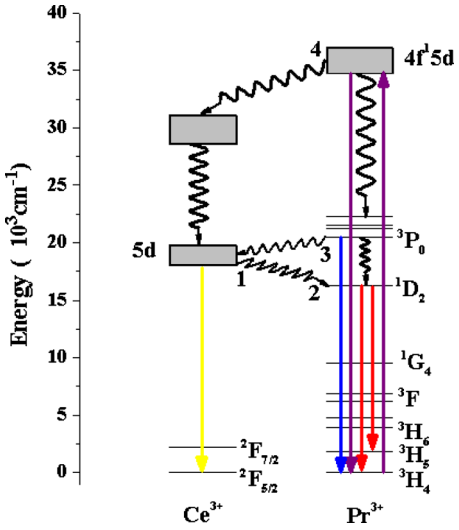

FIG. 15. (Color online) Energy level diagrams of Ce^{3+} and Pr^{3+} with the indicated pathway of $Pr^{3+} \rightarrow Ce^{3+}$ ET.

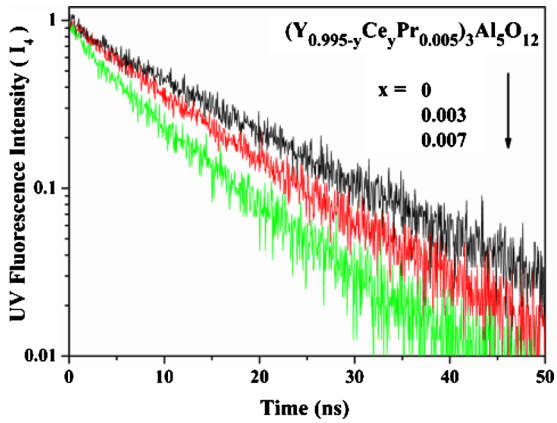

FIG. 16. (Color online) Decay curves of the UV fluorescence of Pr in $(Y_{0.995-y}Ce_yPr_{0.005})_3Al_5O_{12}$ for y=0, 0.003, and 0.007.

disappears at y=0.02. We have experimentally proved that this behavior is due to reabsorption of the blue PL by the lowest 5*d* state of Ce^{3+}. As the 4*f*5*d* of Pr^{3+} is excited, besides the ET to the 5*d* state of Ce^{3+}, part of the excitation energy may relax directly down to the $^3P_0$, which subsequently relaxes down to the lower level $^1D_2$. It is found in Fig. 14 that the totally integrated PL intensities of the whole emission lines from $^3P_0$ and $^1D_2$ are much less than that from the 4*f*5*d* band for y=0. It implies that only a small part of the 4*f*5*d* relaxes down to the lower levels. This conclusion is also supported by the result obtained by Weber[23] that the fluorescent quantum efficiency of the lowest 4*f*5*d* state is near to unity due to a large energy gap ~10 000 cm^{-1} between the lowest 4*f*5*d* and the nearest $^3P_2$ manifold of the 4*f* configuration. Moreover, for each y the $^3P_0$ 5*d* ET efficiency η_{31} is less than the 4*f*5*d*-5*d* ET efficiency η_{41}, as listed in Table II. Therefore, the ET from the $^3P_0$ of Pr^{3+} to the 5*d* of Ce^{3+} can be neglected in comparison with the transfer from the 4*f*5*d* of Pr^{3+} to the 5*d* of Ce^{3+}.

The Pr^{3+}–Ce^{3+} ET leads to the reduction of the UV fluorescence intensity and lifetime with the increase in y. Figure 16 shows the decay curves of the UV fluorescence of Pr^{3+} for various y. The decay for y=0 is purely exponential with the lifetime of 14 ns. In view of near-unity quantum efficiency of the lowest 4*f*5*d* fluorescence,[23] we write the intrinsic lifetime of the lowest 4*f*5*d* state $\tau_{40}=\langle\tau_4\rangle_0=14$ ns. The intrinsic lifetime of the lowest 4*f*5*d* state of Pr^{3+} is quite shorter than the intrinsic lifetime (~61 ns) of the lowest 5*d* state of Ce^{3+}. The decay continue to become faster with increasing y followed by a change from exponential to slightly nonexponential behavior. As y higher than 0.007, the lifetime is about several nanoseconds too short to be measured accurately in the present work. Hence, we present the results of the sample series B with y=0–0.007. Only considering the ET from the lowest 4*f*5*d* of Pr^{3+} to the 5*d* of Ce^{3+}, we obtain a proportional dependence of the yellow/UV ratio (I_1/I_4) on y using Eq. (2) with the measured values of related lifetimes listed in Table II. The calculated proportional dependence of I_1/I_4 is consistent with that obtained directly from the PL spectra (see Fig. 14), as shown in Fig. 17. We can see in Fig. 16 that the decay curves do not deviate from an exponential function very much with increasing y and exhibit approximately ex-

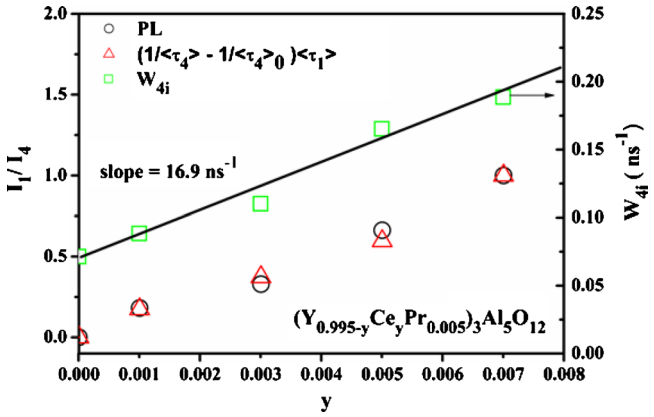

FIG. 17. (Color online) y dependence of ratio (I_1/I_4) obtained directly from PL spectra compared with that evaluated using $(1/\langle\tau_4\rangle - 1/\langle\tau_4\rangle_0)\langle\tau_1\rangle$, where the value of the ratio at y=0.007 is normalized. The y dependence of W_{4i} is also shown.

ponential for y in the range of 0–0.007. In this case, the ET rate keeps at the initial rate during the ET. In general, the initial ET rate increases proportionally with the acceptor concentration as described by Eq. (5), consequently resulting in a linear growth of the yellow/UV ratio with y in the case of approximately exponential decays of donor fluorescence for various y interested in the present work. Looking for the lifetimes listed in Table II, the value of $\langle\tau_4\rangle$ reduces to around half of the τ_{40} as y=0.007, i.e., the macroscopic ET rate $1/\langle\tau_4\rangle - 1/\tau_{40}$ less than the intrinsic radiative rate $1/\tau_{40}$ for y in the range of this work. This reasonably results in an approximately exponential decay of the UV fluorescence in the time scale of τ_{40} (see Fig. 16). The linear dependence of the initial decay rates of the UV fluorescence on y, as shown in Fig. 17, gives the value of $\Sigma_l w_{0l}$ to be 16.9 ns^{-1}, yielding $\tau_{40}\Sigma_l w_{0l}$ to be 237 for ET from the $4f5d$ of Pr^{3+} to the $5d$ of Ce^{3+}. This value is larger than 73 for Ce^{3+}–Pr^{3+} ET but smaller than 1252 for Pr^{3+}–Pr^{3+} ET.

At last, we discuss the change in the intensity of the $^1D_2 \rightarrow {}^3H_4$ red emission line with y in Fig. 14. The red line is stronger for y=0 than that for y=0.001. This is mainly due to a longer lifetime of the $^1D_2$ level for y=0. Subsequently, the red line grows up with increasing y from 0.001 to 0.02. The population of $^1D_2$ may possibly be provided through the followed three ways, the direct feed by the $4f5d$ the relaxation from $^3P_0$ and the ET from Ce^{3+}. To exam the former two processes, the time profiles of the red fluorescence in YAG: 0.005 Pr^{3+} are measured as the $4f5d$ is excited by a pulsed laser at 288 nm and/or the $^3P_0$ is excited by a pulsed laser at 488 nm. The two time profiles are almost identical, exhibiting a rise and decay pattern with the rising time consistent with the lifetime of the $^3P_0$ level. The initial intensity is zero for $^3P_0$ excitation and nonzero but very weak for $4f5d$ excitation. From the time profile for $4f5d$ excitation, we estimated that 92% of the population of the $^1D_2$ is fed by $^3P_0$ and only 8% is fed directly by $4f5d$. With addition of Ce^{3+}, the $4f5d$ of Pr^{3+} may transfer its energy to the $5d$ state of Ce^{3+}, which subsequently transfers to the $^1D_2$ of Pr^{3+}. As a result, the red line enhances with increasing y. Due to the additional feed by $^3P_0$ and $4f5d$ red/yellow intensity ratio upon 288 nm excitation is always higher than that upon $5d$ excitation of Ce^{3+} at 340 nm. For comparison, The PL spectrum of the sample with y=0.02 under 340 nm excitation is also presented in Fig. 14.

IV. CONCLUSION

Nonradiative mutual ETs occur between Ce^{3+} and Pr^{3+} in $Y_3Al_5O_{12}$ (YAG). The $Ce^{3+} \rightarrow Pr^{3+}$ ET starts from the lowest $5d$ state of Ce^{3+} to the $^1D_2$ level of Pr^{3+} rather than the $^3P_0$ state of Pr^{3+}. As the lowest $4f5d$ band of Pr^{3+} is excited at 288 nm, $Pr^{3+} \rightarrow Ce^{3+}$ ET can occur through two pathways. One performs a direct transfer from the lowest $4f5d$ state of Pr^{3+} to the $5d$ state of Ce^{3+}. Another describes that the lowest $4f5d$ state relaxes down to the $^3P_0$ levels which subsequently transfers to the lowest $5d$ state of Ce^{3+}. The former pathway is dominant.

Upon $5d$ excitation of Ce^{3+} in YAG:Ce^{3+}, Pr^{3+}, the Ce^{3+}–Pr^{3+} ET results in a growth of the intensity ratio of the $^1D_2 \rightarrow {}^3H_4$ red line of Pr^{3+} to the yellow band of Ce^{3+} with increasing Pr^{3+} concentration up to a critical concentration. Further increasing Pr^{3+} concentration leads to a reduction of the red/yellow ratio and an rapid shortening of the $^1D_2$ lifetimes due to concentration quenching by a $Pr^{3+} \rightarrow Pr^{3+}$ cross relaxation described by $(^1D_2, {}^3H_4) - (^1G_4, {}^3F_4)$.

An increase in the Ce^{3+}–Pr^{3+} ET rate followed by the enhanced the red/yellow ratio on only increasing Ce^{3+} concentration is observed. This behavior is attributed to the increase in the spectral overlap integrals between Ce^{3+} emission and Pr^{3+} excitation due to the fact that the yellow band shifts to the red side with increasing Ce^{3+} concentration while the red line dose not move.

Ce^{3+}–Pr^{3+} and Pr^{3+}–Pr^{3+} ET are both governed by electric dipole–dipole interaction. For Ce^{3+} concentration of 0.01, the corresponding rate constant and critical distance are evaluated to be 4.5×10^{-36} $cm^6\ s^{-1}$, 0.81 nm for Ce^{3+}–Pr^{3+} ET and 2.4×10^{-38} $cm^6\ s^{-1}$, 1.30 nm for Pr^{3+}–Pr^{3+} ET. Spectroscopic study also demonstrates a pronounced ET from the lowest $4f5d$ of Pr^{3+} to the $5d$ of Ce^{3+}.

A proportional dependence of the initial transfer rate on acceptor concentration is observed in each of these ET pathways. The proportional coefficient as the averaged ET parameters for initial decay are determined to be $73\tau_{10}^{-1}$ for ET from Ce^{3+} lowest $5d$ to Pr^{3+} $^1D_2$, $1252\tau_{20}^{-1}$ for ET from Pr^{3+} $^1D_2$ to another Pr^{3+} in the ground state, and $237\tau_{40}^{-1}$ for ET from Pr^{3+} lowest $4f5d$ to Ce^{3+} $5d$ states, respectively, meaning the ET efficiency for the same concentration of acceptors follows the order of Pr^{3+}–$Pr^{3+} > Pr^{3+}$–$Ce^{3+} > Ce^{3+}$–Pr^{3+}.

The relative PL intensities of Ce^{3+} and Pr^{3+} for various Ce^{3+} and Pr^{3+} concentrations are in good agreement with the results evaluated from fluorescence decay data.

ACKNOWLEDGMENTS

This work is financially supported by the National Nature Science Foundation of China (Grant No. 10834006 (Grant Nos. 10774141, 10904141, 10904140), the MOST of China (Grant no. 2006CB601104), the Scientific project of Jilin province (20090134 and 20090524), and CAS Innovation Program.

[1]G. Blasse and A. Bril, Appl. Phys. Lett. **11**, 53 (1967).
[2]G. Blasse and A. Bril, J. Chem. Phys. **47**, 5139 (1967).
[3]R. Mueller-Mach, G. O. Mueller, M. R. Krames, and T. Trottier, IEEE J. Sel. Top. Quantum Electron. **8**, 339 (2002).
[4]Y. Pan, M. Wu, and Q. Su, J. Phys. Chem. Solids **65**, 845 (2004).
[5]H. S. Jang, W. B. Im, D. C. Lee, D. Y. Jeon, and S. S. Kim, J. Lumin. **126**, 371 (2007).
[6]H. Yang and Y. S. Kim, J. Lumin. **128**, 1570 (2008).
[7]H. Yang, D. K. Lee, and Y. S. Kim, Mater. Chem. Phys. **114**, 665 (2009).
[8]S. K. Gayen, B. Q. Xie, and Y. M. Cheung, Phys. Rev. B **45**, 20 (1992).
[9]G. Özen, O. Forte, and B. Di Bartolo, J. Appl. Phys. **97**, 013510 (2005).
[10]G. Özen, O. Forte, and B. Di Bartolo, Opt. Mater. **27**, 1664 (2005).
[11]M. Malinowski, P. Szczepanski, W. Woliński, R. Wolski, and Z. Frukacz, J. Phys.: Condens. Matter **5**, 6469 (1993).
[12]H. Chen, R. Lian, M. Yin, L. Lou, W. Zhang, S. Xia, and J. C. Krupa, J. Phys.: Condens. Matter **13**, 1151 (2001).
[13]M. Inokuti and F. Hirayama, J. Chem. Phys. **43**, 1978 (1965).
[14]P. M. Selzer, D. L. Huber, B. B. Barnett, and W. M. Yen, Phys. Rev. B **17**, 4979 (1978).
[15]M. M. Broer, D. L. Huber, and W. M. Yen, Phys. Rev. Lett. **49**, 394 (1982).
[16]D. L. Huber, Phys. Rev. B **20**, 5333 (1979).
[17]W. Lenth, G. Huber, and D. Fay, Phys. Rev. B **23**, 3877 (1981).
[18]T. Y. Tien, E. F. Gibbons, R. G. Delosh, P. J. Zacmanidis, D. E. Smith, and H. L. Stadler, J. Electrochem. Soc. **120**, 278 (1973).
[19]M. Yokota and O. Tanimoto, J. Phys. Soc. Jpn. **22**, 779 (1967).
[20]D. L. Huber, Phys. Rev. B **20**, 2307 (1979).
[21]V. Bachmann, C. Ronda, and A. Meijerink, Chem. Mater. **21**, 2077 (2009).
[22]A. A. Setlur, W. J. Heward, and Y. Gao, Chem. Mater. **18**, 3314 (2006).
[23]M. J. Weber, Solid State Commun. **12**, 741 (1973).